JOURNAL OF CATALYSIS 94, 514–530 (1985)

Surface Spectroscopic Characterization of Cu/Al_2O_3 Catalysts

BRIAN R. STROHMEIER,[1,2] DONALD E. LEYDEN,[3] R. SCOTT FIELD,[3] AND DAVID M. HERCULES[1]

Departments of Chemistry, University of Pittsburgh, Pittsburgh, Pennsylvania 15260; and Colorado State University, Ft. Collins, Colorado 80523

Received March 8, 1984; revised March 5, 1985

The surface properties of a series of impregnated Cu/Al_2O_3 catalysts were investigated by a variety of spectroscopic techniques: X-ray photoelectron spectroscopy (ESCA or XPS), low-energy ion scattering spectroscopy (ISS), photoacoustic spectroscopy (PAS), and X-ray diffraction. The surface characteristics of the catalysts are affected by both metal loading and calcination temperature. At low Cu loadings (<10%), copper ions form a well-dispersed interaction species with the support. At higher copper contents, segregation of bulk-line CuO occurs. Reduction by H_2 and sulfidation with 15% H_2S/H_2 (350°C), lead to formation of metallic Cu and Cu_2S, respectively.

INTRODUCTION

Supported copper catalysts are widely used in oxidation reactions, alkane dehydrogenation, and hydrogenation of aldehydes and ketones. Because of the widespread importance of copper catalysts, the Cu/Al_2O_3 system has been studied extensively by a variety of instrumental techniques including X-ray diffraction (XRD) (*1–5*), magnetic susceptibility (*1, 6*), electron spin resonance (ESR) (*3, 5, 7, 8*), diffuse reflectance spectroscopy (DRS) (*1, 3, 6, 9, 10, 14*), thermal analysis (*2, 6, 11*), electron probe microanalysis (*12*), X-ray absorption edge shifts (*3, 5*), extended X-ray absorption fine structure (EXAFS) (*3*), X-ray photoelectron spectroscopy (ESCA or XPS) (*3, 13, 14*), secondary ion mass spectrometry (SIMS) (*15*), and low-energy ion scattering spectroscopy (ISS) (*16*). Despite this extensive characterization, the nature of copper species on catalyst surfaces is essentially not well understood. Inconsistencies between investigators have arisen presumably because of the different sampling depths, and sensitivities of the various techniques used.

The most extensive investigation of Cu/Al_2O_3 catalysts has been performed by Friedman *et al.* (*3*). By applying several techniques and combining results with previous work, a coherent model of the surface structure was developed, resulting in the following conclusions (*3, 14*):

1. At low metal loadings (<4% Cu/100 m^2/g support) and at calcination temperatures below 500°C, formation of a "surface spinel" (which "resembles" $CuAl_2O_4$) predominates. Most of the Cu^{+2} ions are in a distorted octahedral geometry, unlike bulk $CuAl_2O_4$ where about 60% are tetrahedral and 40% octahedral.

2. At higher metal loadings, segregation of bulk-like CuO may also occur.

3. Calcination at 900°C leads to formation of bulk $CuAl_2O_4$.

Hence, it appears that both metal loading and calcination temperature are key factors in determining the extent of metal–support interaction.

The present study is aimed toward elucidation of the Cu surface species formed on the oxidic catalysts as a function of metal loading (1–26% Cu) and calcination temper-

[1] University of Pittsburgh.

[2] Present address: Center for Catalytic Science and Technology, University of Delaware, Newark, Del. 19716.

[3] Colorado State University.

0021-9517/85 $3.00

ature (400 or 600°C). The surface spectroscopic techniques of ESCA and ISS, as well as the "bulk" techniques of XRD and photoacoustic spectroscopy (PAS) have been employed to characterize the nature of the catalysts. Although the Cu/Al_2O_3 system has been studied extensively, the use of surface-sensitive techniques such as ESCA and ISS has been limited and mostly inconclusive, prompting the present study. In addition to the spectroscopic investigation, reactivity of the catalysts to H_2 reduction and H_2S/H_2 sulfidation was evaluated, with emphasis on the surface species formed by these treatments.

This study differs from the earlier work of Friedman *et al.*; in their study major emphasis was on only a few metal loadings (ca. 3, 6, 9, and 16% Cu) at different calcination temperatures (500 or 900°C) on alumina supports having different surface areas (165 and 75 m^2/g). However, the results presented here are in qualitative agreement with their main conclusions given above.

EXPERIMENTAL

Catalyst preparation. Two series of Cu/Al_2O_3 catalysts were prepared by wet impregnation of γ-Al_2O_3 (Harshaw Chemical Co., Alumina No. AL-1401P; BET surface area: 195 m^2/g) with an aqueous copper(II) nitrate solution. Excess water was evaporated at 90° with stirring. The samples were dried for 24 h at 110°C, finely ground, and subsequently calcined in dry air for 5 h at either 400 or 600°C. $Cu(NO_3)_2$ decomposed completely after calcination, as indicated by the lack of a N 1*s* signal in the wide-scan ESCA spectra of the catalysts. The catalysts exhibited a wide variety of colors ranging from pale blue (≤2% Cu), to blue–green (3–8% Cu), to olive green (10 to 17% Cu), to black (>17% Cu).

Standard materials. All reference compounds with the exception of $CuAl_2O_4$ were purchased from Cerac Inc. and were used without further purification. XRD patterns of all reference compounds exactly matched the appropriate ASTM powder diffraction file; no stray lines were present.

$CuAl_2O_4$ was prepared (*17*) by mixing stoichiometric amounts of $Cu(NO_3)_2 \cdot 6H_2O$ and $Al_2(SO_4)_3 \cdot 18H_2O$ in distilled water and heating at 110°C until dry. The resultant mixture was finely ground and subsequently calcined for 5 h at 950°C. XRD patterns of the brown product indicated the presence of bulk $CuAl_2O_4$, as well as a small amount of unreacted CuO. Therefore, the product was repeatedly washed with 1 *M* $(NH_4)_2CO_3$ to remove the unreacted CuO (*4*), rinsed with distilled water, filtered, and dried overnight at 110°C. XRD patterns of the washed product showed only lines corresponding to $CuAl_2O_4$.

ESCA spectra. ESCA spectra were obtained with an AEI ES200A electron spectrometer equipped with an AEI DS100 data system interfaced to an Apple II plus (48K) microcomputer. The spectrometer utilizes nonmonochromatized Al*Kα* radiation (1486.6 eV). The anode was operated at 12 kV and 22 mA. The instrument typically operates at pressures below 5×10^{-8} Torr. Samples were mounted in the form of a powder on a water-cooled aluminum probe using Scotch brand double-sided tape.

ESCA binding energies and intensity ratios are the averages of at least three separate determinations. For catalyst samples, the Al 2*p* line (74.5 eV) of the alumina support was used as an internal reference for determination of binding energies. The binding energy of the Al 2*p* line was determined by vacuum deposition of gold on γ-Al_2O_3, referencing to the Au $4f_{7/2}$ line (83.8 eV). The average C 1*s* binding energy found on γ-Al_2O_3 and all catalyst samples was 285.1 eV. Therefore, binding energies for all standard compounds were referenced to the C 1*s* value of 285.1 eV. ESCA intensity ratios were determined using the total integrated areas of the Cu $2p_{3/2}$ (and associated satellites) and the Al 2*p* photoelectron lines. (Note: the Cu 3*p* line overlaps the Al 2*p* line; hence the Cu 3*p* intensity was un-

avoidably included in calculating the Cu/Al intensity ratios). In the peak area computation, the background was assumed to be linear over the peak width. Intensity ratios were reproducible to ±10% (r.s.d.) or better.

ISS spectra. ISS spectra were recorded using a 3M Model 525/610 ISS/SIMS spectrometer, which employs a cylindrical mirror analyzer (CMA) to measure the energy of the backscattered ions. Monoenergetic $^4He^+$ ions were used with a primary ion energy of 2 kV and a current density of ca. 2×10^{-7} A/cm^2, corresponding to a sputtering rate of approximately 4 monolayers per hour. A typical base pressure of 5×10^{-9} Torr was achieved before helium was admitted to the spectrometer. Spectra were obtained with a helium pressure in the sample chamber of 2.0×10^{-5} Torr. Samples (ca. 50 mg) were pressed into pellets (6 × 15 mm) at approximately 5000 psi and mounted on an aluminum probe with double-sided tape. Charge neutralization was accomplished by thermal electron emission from a resistively heated thoriated tungsten filament operated at 2 mA. The E/E_0 region from 0.3 to 1.0 was recorded with a scan time of approximately 3 min. ISS intensity ratios were determined using Cu and Al peak heights, measured manually assuming a linear background over the peak width. Peak height intensity ratios reported are the averages of at least three determinations. Intensity ratios were measured with a precision of ±10% or better.

Photoacoustic spectra. Photoacoustic characterization was performed at Colorado State University; the spectrometer, data analysis method, and calibration procedure have been described previously (*18*). Optical spectra in the visible region were obtained with a xenon arc lamp operated at 300 W. The typical modulation frequency was 177 Hz. Air was used exclusively as the coupling gas. Normalization of data was performed against the PAS spectrum of carbon black.

X-Ray diffraction. X-Ray powder diffraction patterns were obtained at room temperature using a Diano Model 700 diffractometer employing Ni-filtered Cu$K\alpha$ radiation (1.54056 Å). The X-ray tube was operated at 50 kV and 25 mA. Samples were finely ground and packed into a plastic holder having an 18 × 18 × 2-mm opening. No adhesive or binder was necessary. Spectra were scanned at a rate of 0.4° min^{-1} (in 2θ).

Determination of the CuO crystallite size was based on X-ray diffraction line broadening. The mean crystallite size (d) was calculated from the Scherrer equation (*19*):

$$d = \frac{K\lambda}{\beta \cos \theta},$$

where λ is the X-ray wavelength (1.54056 Å), K is the Scherrer constant (particle shape factor), taken as unity, and β is the full width at half maximum (FWHM), in radians, of the CuO ⟨111⟩ line (35.6° in 2θ). Reported crystallite sizes were corrected for instrumental broadening as described by Klug and Alexander (*19*). Because of signal-to-noise considerations, accurate measurement of the FWHM's was possible only for catalysts having copper concentrations of 17% or greater.

Chemical analysis. Bulk Cu concentrations (wt%) were determined by atomic absorption spectroscopy using a Perkin–Elmer Model 2380 A.A. spectrophotometer. Catalyst samples were dissolved by digestion in concentrated sulfuric acid. For the sake of simplicity, all metal concentrations are reported as integral values. Actual concentrations are within ±0.2% (absolute) of the nominal values.

Chemical reactions. All samples were pressed into pellets prior to gas-phase reactions. To confirm that the pelleting process did not induce chemical changes in the catalysts, the ESCA binding energies and Cu/Al intensity ratios for samples dusted onto double-sided tape were compared with the values obtained for samples pressed as pellets. No differences were observed within

experimental error; hence, it was assumed that the original powdered catalysts were identical with the pressed catalysts.

Samples were mounted on an air-cooled sealable probe with stainless-steel clips. The probe allows transfer of samples from the reaction chamber to the ESCA spectrometer without exposure to air. The probe and reaction chamber have been described previously (*20, 21*). The sample probe was inserted into the reaction chamber in the sealed position, while the reaction chamber was heated to the desired temperature and allowed to equilibrate under gas flow (50 ml/min). Once the desired temperature was reached (ca. 30 min), the probe was opened and the reaction was allowed to proceed for a specified length of time. After the reaction was completed, the probe was closed, allowed to cool, and then transferred to the spectrometer.

For reduction studies, pure H_2 (99.999%) was employed (Air Products). Sulfidation was accomplished with 15% H_2S/H_2 (Air Products). All gases were used as received without further purification.

RESULTS

Bulk and Surface Characterization of Oxidic Cu/Al_2O_3

XRD results. The two major diffraction peaks for bulk CuO are located at 35.6° and 38.8° in 2θ ($CuK\alpha$ radiation). This region is therefore convenient for determining the presence of bulk-like CuO on catalysts. There is difficulty, however, in detecting bulk aluminate formation because both $CuAl_2O_4$ and γ-Al_2O_3 are spinel-type phases, and their diffraction peaks nearly coincide (*3*).

The γ-Al_2O_3 support gave broad diffuse diffraction lines, indicating poor crystallinity. For Cu loadings below 13%, XRD patterns of the catalysts (both 400 and 600°C calcination) were essentially identical to the support pattern, indicating highly dispersed or amorphous Cu species. This finding is consistent with previously reported results

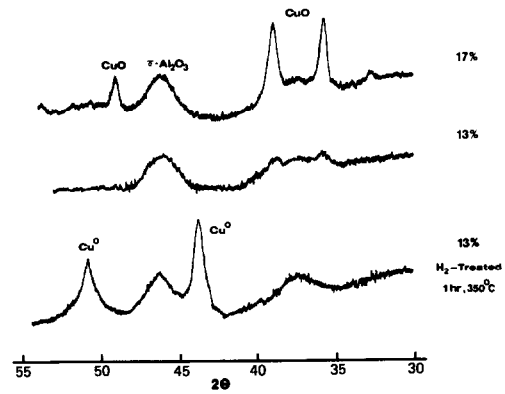

FIG. 1. XRD patterns of various Cu/Al_2O_3 catalysts (600°C): 17% Cu/Al_2O_3, 13% Cu/Al_2O_3, H_2-treated 13% Cu/Al_2O_3.

(*3, 5*). However, for Cu loadings of 13% or more, XRD patterns of the catalysts (both 400 and 600°C) indicated the presence of CuO as shown in Fig. 1. The intensities of the CuO diffraction lines increased linearly (relative to the major γ-Al_2O_3 line at 46.0°, 2θ) with Cu loading (>13%), indicating build-up of a CuO phase on the catalysts. Formation of bulk CuO at high Cu loadings (≥13%) can be attributed to agglomeration of Cu species, presumably due to saturation of the support. The black color of catalysts containing greater than 17% Cu is consistent with formation of a CuO phase.

The calculated CuO crystallite sizes are listed in Table 1. The results show that in general, there is an increase in the CuO crystallite size with increasing metal loading and/or calcination temperature. However, it must be noted that while X-ray line broadening measurements are useful as a relative measure of average crystallite size, the Scherrer formula should not be used for absolute determinations due to its failure to account for the effects of microstrain, the consequences of particle size distribution, and the uncertainty in correcting for instrumental broadening. Hence, the values listed in Table 1 are meant to be used for relative comparisons only.

PAS results. Optical spectra of species on the surfaces of supported catalysts can provide a great deal of information about

TABLE 1

Crystallite Sizes of Cu/Al_2O_3 Catalysts (Å × 10^{-2})[a]

Catalyst[b]	Calcination temperature	
	400°C	600°C
17% Cu	1.8	2.9
22% Cu	2.8	3.5
26% Cu	3.2	3.9

[a] Determined by X-ray diffraction line broadening of the CuO ⟨111⟩ line.

[b] Because of signal to noise considerations, accurate measurement of the FWHM's was possible only for catalysts having Cu concentrations of 17% or greater.

their identity. This type of information has been obtained primarily through diffuse reflectance spectroscopy (DRS). PAS and DRS give the same general information since the spectra result from the same electronic processes for both techniques. However, the application of PAS to the study of catalysts has been exploited to only a limited extent (*21, 22*). Since PAS is relatively insensitive to light scattering by the sample, it is potentially more suitable for studying supported catalysts than DRS.

The interaction of Cu(2+) ions with γ-Al_2O_3 has been studied extensively using DRS (*1, 3, 6, 9, 10*). The Cu/Al_2O_3 system shows two main absorption bands due to Cu(2+) in octahedral (Oh) and tetrahedral (Td) geometries, with the maxima located, respectively, in the absorption regions between 750–800 and 1400–1600 nm (*3, 6, 9, 10*).

The PAS spectrum of $CuAl_2O_4$ showed a broad band from 400 to ca. 650 nm in good agreement with DRS spectra of $CuAl_2O_4$ in the visible region (*3, 9*). This band has been attributed to a charge transfer process (*9*). This charge transfer band obscures the presence of any discrete peaks due to Oh Cu(2+) (*9*). The PAS spectrometer used in this study operates in the range 350–750 nm; hence, the Td absorption band of $CuAl_2O_4$ could not be observed. The spectrum of CuO was rather featureless and characteristic of signal saturation, which occurs when the sample acts as a blackbody absorber. Cu_2O showed a weak absorption edge from ca. 600–650 nm, with an absorption band extending to 400 nm.

PAS spectra of Cu/Al_2O_3 catalysts ($\leq$17% Cu) showed weak absorption above 550 nm consistent with DRS results reported previously (*3, 9*) and characteristic of Cu(2+) ions in Oh sites of γ-Al_2O_3. For black catalyst samples (>17% Cu), the spectra were essentially featureless. (Spectra of catalysts calcined at 600°C were essentially identical to the spectra of catalysts calcined at 400°C.) The poor quality of the spectra ($\geq$17% Cu) suggested that signal saturation was being approached, or that masking of the Cu(2+) Oh band by a stronger absorber was occurring. This would occur if a copper species were formed having a very high absorption coefficient (i.e., CuO). Because of the high absorption coefficient of CuO, its presence in even small quantities would cause a general degradation of the PAS spectrum.

ESCA results. The ESCA binding energies of a variety of copper reference compounds and the γ-Al_2O_3 support are summarized in Table 2. CuO and $CuAl_2O_4$ are useful reference compounds to model the extreme situations which may exist on oxidic Cu/Al_2O_3 catalysts. Cu_2O, Cu^0, $CuSO_4$, and Cu_2S are useful model compounds for reduction and sulfiding studies. It must be noted, however, that although the observed binding energies for catalysts may be close to those of bulk compounds, it does not mean that these compounds are necessarily present on the catalyst surface.

The Cu $2p_{3/2}$ and Cu $L_3M_{4,5}M_{4,5}$(LMM) Auger lines for $CuAl_2O_4$, CuO, Cu_2O, and Cu^0 are shown in Fig. 2. The Cu $2p_{3/2}$ binding energies and bandshapes for $CuAl_2O_4$ and CuO differ, with $CuAl_2O_4$ having the more intense shake-up structure (940–945 eV). The ratio of the satellite intensity to

TABLE 2

ESCA Binding Energies (eV)[a,b] of Reference Compounds

Sample	Cu $2p_{3/2}$	Cu LMM auger[c]	Auger parameter[d]	Cu $2p_{1/2}$	O 1s	Al 2p	Al 2s	S 2p	S 2s
γ-Al_2O_3	—	—	—	—	531.3(3.0)[e]	74.5(2.7)	119.3(3.2)	—	—
$CuAl_2O_4$	935.0(3.1)	916.5	364.9	954.9(3.4)	531.1(2.2)	74.5(2.5)	119.3(2.5)	—	—
CuO	934.1(3.4)	917.5	365.0	954.2(3.5)	530.3(2.4)	—	—	—	—
Cu_2O	932.6(1.7)	916.5	362.5	952.6(2.2)	530.8,531.9	—	—	—	—
Cu	932.6(1.4)	918.5	364.5	952.4(1.9)	—	—	—	—	—
$CuSO_4$	936.3(4.4)	915.2	364.9	956.2(4.8)	532.5(2.1)	—	—	169.8(2.5)	233.4(3.0)
Cu_2S	933.2(1.7)	916.7	363.3	953.1(2.2)	—	—	—	162.9(2.5)	226.9(2.7)

[a] Binding energies (B.E.'s) were measured with a precision of ±0.15 eV or better.
[b] All B.E.'s referenced to C 1s = 285.1 eV.
[c] Auger values in kinetic energy (K.E.) (eV). LMM refers to $L_3M_{4,5}M_{4,5}$.
[d] K.E. (LMM Auger) − K.E. (Cu $2p_{3/2}$ photoelectron), see Ref. (*24*).
[e] Values in parentheses are full width at half maximum (FWHM) (±0.2 eV).

that of the main photoelectron line was found to be 1.10 for $CuAl_2O_4$ and 0.45 for CuO (±10%, r.s.d.). The Auger peaks for $CuAl_2O_4$ and CuO also show a chemical shift. However, although the chemical shifts between the Cu $2p_{3/2}$ and Cu LMM Auger lines for CuO and $CuAl_2O_4$ are 0.9 and 1.0 eV, respectively (see Table 2), the Auger parameters (*24*) (kinetic energy of the LMM Auger line-kinetic energy of the Cu $2p_{3/2}$ photoelectron line) for both compounds are the same within experimental error. Hence, Auger parameters cannot be used to distinguish between CuO and $CuAl_2O_4$ on catalysts.

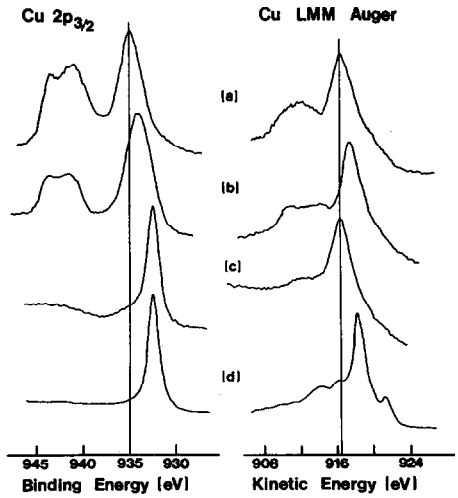

FIG. 2. ESCA spectra of the Cu $2p_{3/2}$ and Cu LMM Auger lines for copper reference compounds: (a) $CuAl_2O_4$; (b) CuO; (c) Cu_2O; (d) Cu^0.

Cu_2O and Cu^0 are both easily distinguishable from CuO and $CuAl_2O_4$, because of their different binding energies (see Table 2) and lack of shake-up satellite peaks (see Fig. 2). The satellite structure of Cu(2+) compounds (d^9) has been attributed to either $3d \rightarrow 4s$ or ligand-to-metal (O $2p \rightarrow$ Cu $3d$) transitions (*25, 26*). Such transitions are not seen for Cu(1+) compounds or $Cu^0(d^{10})$. In addition, the FWHM's of the CuO and $CuAl_2O_4$ Cu $2p_{3/2}$ lines are about twice that of either Cu_2O or Cu^0 (see Table 2). This broadening has been attributed to multiplet splitting in Cu(2+) compounds (*25*). The Cu $2p_{3/2}$ binding energies and bandshapes cannot be used to distinguish between Cu_2O and Cu because they are essentially identical. However, the Cu LMM Auger lines of Cu_2O and Cu^0 are separated in energy by 2.0 eV and have very different bandshapes, allowing easy distinction between the two species.

It would appear from the results shown in Table 2 and Fig. 2, that the binding energies of the Cu $2p_{3/2}$ and LMM Auger lines could be used to distinguish between $CuAl_2O_4$ and CuO on the surface of Cu/Al_2O_3 catalysts. However, ESCA spectra of the catalysts indicate otherwise. The ESCA binding energies of the catalysts studied are listed in Table 3. The average ESCA binding ener-

TABLE 3

Cu/Al_2O_3 Catalysts: ESCA Results[a,b]

Sample	Calcination temperature			
	400°C		600°C	
	Cu $2p_{3/2}$	Satellite intensity[c]	Cu $2p_{3/2}$	Satellite intensity
1% Cu	934.8(4.9)[d]	0.40	934.2(4.0)	0.39
2% Cu	934.7(4.2)	0.39	934.0(4.0)	0.38
3% Cu	934.4(3.9)	0.39	934.2(4.2)	0.40
4% Cu	934.6(3.8)	0.43	934.1(4.2)	0.37
5% Cu	934.3(4.0)	0.43	934.0(3.9)	0.39
6% Cu	934.5(4.0)	0.42	934.3(4.0)	0.39
7% Cu	934.6(3.6)	0.43	934.5(4.0)	0.43
9% Cu	934.6(3.6)	0.41	934.6(3.8)	0.47
11% Cu	934.6(3.5)	0.51	934.5(3.9)	0.46
13% Cu	934.6(3.6)	0.55	934.5(3.9)	0.41
17% Cu	934.7(4.0)	0.54	934.1(4.3)	0.41
22% Cu	934.0(4.4)	0.44	934.0(4.2)	0.42
26% Cu	934.0(4.5)	0.47	934.1(4.5)	0.44
CuO	934.1(3.4)	0.45		
$CuAl_2O_4$	935.0(3.1)	1.10		

Note. All catalysts showed the following av. B.E.'s: C 1*s*, 285.1(2.7); O 1*s*, 531.2(3.0); Al 2*s*; 119.3(3.1).

[a] All B.E.'s (eV) referenced to Al $2p$ = 74.5 eV.

[b] Cu $2p_{3/2}$ B.E.'s were measured with a precision of ±0.4 eV or better (other reported B.E.'s ±0.15 eV or better).

[c] Cu $2p_{3/2}$ satellite intensity relative to main photoelectron line, ±10% (r.s.d.).

[d] Values in parentheses are full width at half maximum (FWHM) ±0.2 eV.

gies of the Cu $2p_{3/2}$ line for catalysts calcined at either 400 or 600°C vary with sample and lie between the values obtained for CuO and $CuAl_2O_4$. In addition, repeated measurements of the same catalyst were found to vary by as much as ±0.4 eV, except at high loadings (>17%). At high Cu loadings, the Cu $2p_{3/2}$ binding energies were reproducible to ±0.10 eV and were characteristic of CuO (see Table 3). On all catalyst samples, other photoelectron lines (i.e., Al 2*s*, O 1*s*, C 1*s*) showed variation of only ±0.15 eV. The observed variation in the Cu $2p_{3/2}$ binding energy is consistent with the results of Friedman *et al.* (*3*) and is behavior characteristic of a surface having mixed species, or possibly the result of differential charging. In addition, it was difficult to assign accurate binding energies to the Cu LMM Auger lines, because the peaks were non-Gaussian and very broad due to high background of the catalyst spectra. Some representative catalyst spectra are shown in Fig. 3.

The variation in binding energies observed for the Cu $2p_{3/2}$ and Cu LMM lines may be partially due to the fact that some Cu(2+) compounds can undergo reduction to Cu(1+) during ESCA experiments (*27–29*). It has been shown that CuO is readily reduced to Cu_2O on heating under vacuum (*27–30*); however, $CuAl_2O_4$ shows no noticeable reduction under these conditions (*29, 30*). The reduction phenomenon has been attributed to factors such as X-ray flux, X-ray dose, temperature, and vacuum pressure. The most recent study, has shown that the decomposition of Cu(2+) compounds arises from sample heating in the spectrometer (*29*). In this study, such

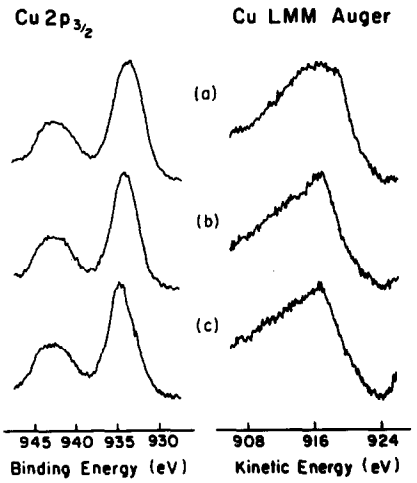

FIG. 3. ESCA spectra of the Cu $2p_{3/2}$ and Cu LMM Auger lines for Cu/Al_2O_3 catalysts: (a) 26% Cu, 600°C; (b) 13% Cu, 400°C; (c) 4% Cu, 400°C.

effects were minimized by water cooling the ESCA probe. Although it has been shown that Cu/Al_2O_3 catalysts can undergo surface reduction on heating under vacuum (*6, 14, 30*), no noticeable reduction occurred on the catalyst samples under the experimental conditions typically employed in this study.

Consistent with the results of Ertl *et al.* (*14*), we have also found (*30*) that Cu/Al_2O_3 catalysts undergo surface reduction (to Cu_2O) on heating under vacuum (275°C). However, the extent of reduction was significantly less than that of bulk CuO under the same experimental conditions (*6, 14, 30*). This lowered reducibility implies that on Cu/Al_2O_3 catalysts, the Cu(2+) ions have interacted with and are bound to the support. This postulate is supported by the fact that bulk $CuAl_2O_4$ does not reduce on heating under vacuum (*29, 30*). In addition, the fact that the interaction species reduces partially, indicates that this species also differs from bulk $CuAl_2O_4$ to some extent.

It was noted earlier that the Cu $2p_{3/2}$ satellite structure of $CuAl_2O_4$ was more intense than that of CuO. Hence, since the Cu $2p_{3/2}$ binding energies of the catalysts varied, giving little information, the satellite intensities were measured to indicate which species were present on the catalysts. The Cu $2p_{3/2}$ satellite intensities (relative to the main Cu $2p_{3/2}$ photoelectron line) obtained for the catalysts are listed in Table 3. Table 3 shows that for all catalysts studied, the satellite intensities were within experimental error of the value obtained for CuO. This result is not surprising for catalysts containing high Cu loadings (>13%) on which bulk CuO was detected by XRD. However, since the satellite intensities for catalysts with low loadings were also within experimental error of that for CuO, it implies that the dispersed copper species is different from $CuAl_2O_4$.

The [Cu $2p_{3/2}$ (+ satellites)]/Al $2p$ ESCA intensity ratio plotted as a function of bulk copper content is shown in Fig. 4 for catalysts calcined at 400 and 600°C. The Cu/Al intensity ratio increased linearly with Cu content up to approximately 9–10% Cu, above which, the curves leveled off. The drastic change in slope indicates an alteration in surface composition at about 9–10% Cu. At all concentrations, the Cu/Al intensity ratios are slightly larger for catalysts calcined at 400°C than for those calcined at 600°C.

ISS results. The Cu/Al ISS intensity ratio is influenced by both copper content and

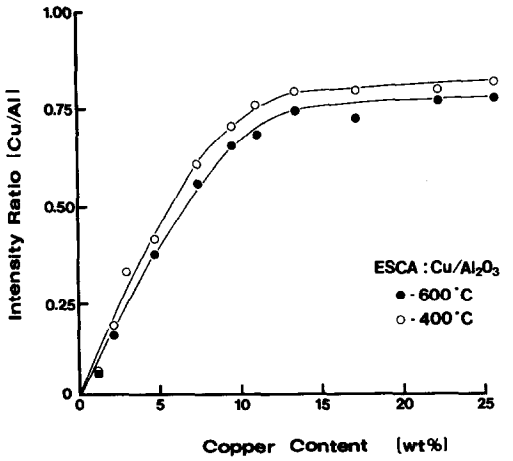

FIG. 4. ESCA Cu $2p_{3/2}$/Al $2p$ intensity ratio vs bulk copper content at different calcination temperatures: (●) 400°C; (○) 600°C. (Relative ESCA Cu/Al intensity ratio of 1.0 = Cu/Al atomic ratio of ca. 0.03 (*44*).)

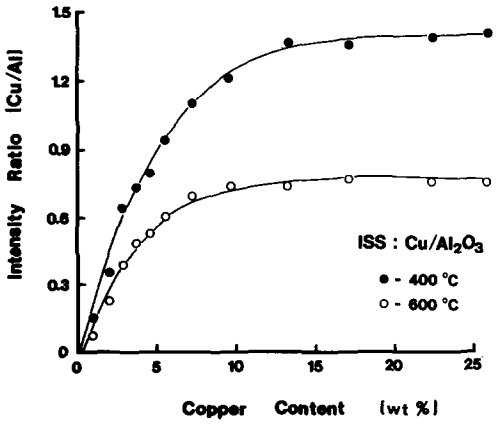

FIG. 5. ISS Cu/Al peak height intensity ratio vs bulk copper content at different calcination temperatures: (●) 400°C; (○) 600°C. (Relative ISS Cu/Al intensity ratio of 1.0 = Cu/Al atomic ratio of ca. 0.2 (*45*).)

calcination temperature. The Cu/Al ISS intensity ratio plotted as a function of copper content is shown in Fig. 5 for catalysts calcined at 400 and 600°C. The results are consistent with the ESCA data. The Cu/Al intensity ratio increases with copper content up to approximately 9–10% Cu. Above 10% Cu, there is a drastic leveling off in the slopes of the curves, indicating a change in surface composition. Figure 5 also shows that the Cu/Al intensity ratios for catalysts calcined at 400°C are significantly larger than for catalysts calcined at 600°C. It is important to note that ISS shows a much larger difference in the Cu/Al intensity ratio with calcination temperature than does ESCA (compare Figs. 4 and 5), illustrating the value of ISS in catalyst studies. This difference can be attributed to the differences in sampling depth between ISS (3 Å) and ESCA (30 Å).

Reduction Studies

Reduction characteristics of supported metal oxides are often quite different from those of bulk oxides because of metal–support interactions and changes in dispersion. Hence, it was of interest to investigate the reducibility of Cu/Al_2O_3 catalysts. In this study, H_2 reduction was carried out at 350°C for 1 h.

To evaluate and compare reactivities of the catalysts, the reduction properties of bulk CuO and $CuAl_2O_4$ were determined. Table 4 lists the Cu $2p_{3/2}$ binding energies and the Cu Auger parameters for reduced CuO and $CuAl_2O_4$. Included for comparison are the values obtained for metallic Cu and Cu_2O. Following reduction, the Cu $2p_{3/2}$ lines for both CuO and $CuAl_2O_4$ showed no satellite peaks characteristic of Cu(2+). The peaks became narrower having FWHM values of 1.8 ± 0.2 eV, and had binding energies characteristic of either Cu_2O or Cu^0 (see Table 4). As seen in Table 4, the Cu Auger parameters indicated that Cu^0 was the species formed by H_2 reduction of CuO and $CuAl_2O_4$. In addition, XRD patterns of reduced CuO and $CuAl_2O_4$ showed only lines corresponding to Cu^0 (major Cu^0 diffraction lines at ca. 43.3° and 50.4°, in 2θ).

Cu/Al_2O_3 catalysts were also found to be reduced easily under the conditions employed regardless of metal loading or calcination temperature, consistent with results reported previously (*6, 10, 11, 14*). Table 5 shows the Cu $2p_{3/2}$ binding energies and Cu $2p_{3/2}$/Al $2p$ intensity ratios for select reduced catalysts. ESCA spectra of the Cu $2p_{3/2}$ line of reduced catalysts showed no evidence of Cu(2+) (for example compare Figs. 6a and b) and the binding energies

TABLE 4

ESCA Results[a] for Reduced and Sulfided Reference Compounds

Sample/Treatment[b]	Cu $2p_{3/2}$	Cu Auger parameter	S $2p$	Cu $2p_{3/2}$/S $2p$[c]
CuO/H_2	932.7	364.4	—	—
$CuAl_2O_4/H_2$	932.6	364.3	—	—
Cu^0	932.6	364.5	—	—
Cu_2O	932.6	362.5	—	—
$CuO/H_2S/H_2$	932.9	363.4	162.7	2.81
$CuAl_2O_4/H_2S/H_2$	933.0	363.3	162.7	2.48
Cu_2S	933.2	363.3	162.9	2.75
$CuSO_4$	936.3	364.9	169.8	1.70

[a] B.E.'s in eV (±0.2 eV).
[b] Treatment for 1 h at 350°C.
[c] All intensity ratios were measured with a precision of ±10% (r.s.d.) or better.

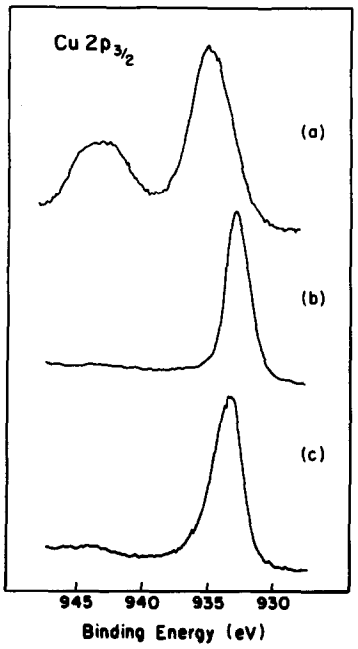

FIG. 6. Cu $2p_{3/2}$ ESCA spectra of 13% Cu/Al_2O_3 (600°C): (a) oxidic state; (b) following H_2 reduction for 1 h at 350°C; (c) following 15% H_2S/H_2 sulfidation for 1 h at 350°C.

were characteristic of either Cu_2O or Cu^0 (see Table 5). The same result was obtained even for reduction treatments as mild as 10% H_2/N_2 for 1 h at 250°C. The Cu $2p_{3/2}$/Al ESCA intensity ratios for reduced catalysts decreased approximately 40% compared to the corresponding oxidic catalyst (see Table 5), indicating a decrease in Cu dispersion on reduction. A decrease in dispersion would arise from sintering of Cu species during reduction, forming larger Cu metal particles.

XRD patterns of reduced catalysts showed lines corresponding to Cu^0 (and γ-Al_2O_3) for catalysts containing 5% Cu or more (for example, see Fig. 1). There was no evidence for other Cu species. Reduced catalysts containing less than 5% Cu showed only γ-Al_2O_3 by XRD. Since XRD did not show the presence of bulk Cu compounds on oxidic catalysts containing less than 13% Cu, the appearance of Cu^0 peaks for reduced catalysts containing 5% Cu, indicates an increase in particle size on reduction, consistent with the ESCA intensity ratio results.

Sulfiding Studies

It is well known that copper-containing catalysts used for methanol synthesis are susceptible to poisoning by sulfur compounds (*31*). In contrast, it has been reported that for acid-catalyzed reactions, the activities of various supported catalysts, including Cu/Al_2O_3, were enhanced by pretreatment with H_2S (*32*). Hence, the reactivity of Cu/Al_2O_3 catalysts toward sulfur compounds is of interest. In this study, sulfidation was accomplished with a 15% H_2S/H_2 mixture at 250°C for 1 h.

To evaluate and compare reactivities of the catalysts, the sulfiding properties of bulk CuO and $CuAl_2O_4$ were determined. Table 4 lists the Cu $2p_{3/2}$ binding energies, Cu Auger parameters, S 2*p* binding energies, and Cu $2p_{3/2}$/S 2*p* intensity ratios for CuO and $CuAl_2O_4$ following sulfidation. Included for comparison are the values obtained for bulk Cu_2S and $CuSO_4$. ESCA spectra of the Cu $2p_{3/2}$ lines of sulfided CuO and $CuAl_2O_4$ showed no evidence of any Cu(2+) species. The Cu $2p_{3/2}$ and S 2*p* binding energies, Cu Auger parameters, and Cu $2p_{3/2}$/S 2*p* intensity ratios obtained for both samples were within experimental error of the values obtained for Cu_2S (see Table 4). XRD patterns of sulfided CuO and $CuAl_2O_4$ showed lines corresponding to CuO + Cu_2S and $CuAl_2O_4$ + Cu_2S, respectively; hence,

TABLE 5

ESCA Results[a] for H_2 Reduced Cu/Al_2O_3 Catalysts

Sample	Reduced catalysts[b]		Oxidic catalysts[c]
	Cu $2p_{3/2}$	Cu $2p_{3/2}$/Al 2*p*	Cu $2p_{3/2}$/Al 2*p*
5% Cu (600°C)	932.9	0.31	0.40
9% Cu (400°C)	932.7	0.48	0.78
13% Cu (400°C)	932.6	0.32	0.75
13% Cu (600°C)	932.9	0.42	0.78
26% Cu (600°C)	932.9	0.45	0.76

[a] ESCA B.E.'s (eV) were reproducible to ±0.2 eV or better.
[b] Treatment for 1 h at 350°C.
[c] ESCA intensity ratios were reproducible to ±10% (r.s.d.) or better.

TABLE 6

ESCA Results[a] for 15% H_2S/H_2 Sulfided Cu/Al_2O_3 Catalysts

Sample	Sulfided catalysts[b]					Oxidic catalysts Cu $2p_{3/2}$/Al 2p
	Cu $2p_{3/2}$	Cu Auger parameter	S 2p	Cu $2p_{3/2}$/S 2p	Cu $2p_{3/2}$/Al 2p	
5% Cu (600°C)	932.9	363.2	163.2	2.17	0.42	0.40
9% Cu (400°C)	932.8	363.3	162.9	2.29	0.70	0.73
13% Cu (400°C)	932.7	363.4	163.2	2.15	0.73	0.75
13% Cu (600°C)	932.7	363.4	162.9	2.10	0.72	0.78
16% Cu (600°C)	932.7	363.5	163.4	2.45	0.71	0.76

[a] ESCA B.E.'s (eV) were reproducible to ±0.2 eV.
[b] Treatment for 1 h at 350°C.
[c] ESCA intensity ratios were reproducible to ±10% (r.s.d.) or better.

sulfidation was not complete under the conditions employed. However, the results indicate that at least within the sampling depth of ESCA, all Cu(2+) species were converted to Cu_2S.

The reactivity to sulfiding of Cu/Al_2O_3 catalysts was similar to the reactivity of CuO and $CuAl_2O_4$, independent of Cu loading or calcination temperature. ESCA spectra of the Cu $2p_{3/2}$ lines of sulfided catalysts showed no evidence of any Cu(2+) species (for example, compare Figs. 6a and c). The Cu $2p_{3/2}$ and S 2p binding energies of the catalysts varied somewhat, but were within 0.5 eV of the values obtained for Cu_2S (see Tables 4 and 6). This large difference was presumably caused by charging on the catalysts. Unlike the results observed for oxidic catalysts, the Auger lines of sulfided catalysts were sufficiently intense to be measured accurately. The Auger parameters obtained for sulfided catalysts were identical with Cu_2S within experimental error (±0.2 eV) (see Tables 4 and 6). Also, the Cu $2p_{3/2}$/S 2p intensity ratios for sulfided catalysts (see Table 6) were characteristic of Cu_2S. In contrast to the reduction studies, the Cu $2p_{3/2}$/Al 2p intensity ratios for sulfided catalysts were within experimental error of the values obtained for the corresponding oxidic catalysts (see Table 6). This indicates that there was no major change in dispersion of Cu species on sulfidation.

XRD patterns of sulfided catalysts containing greater than 5% Cu indicated only the presence of Cu_2S and γ-Al_2O_3. It appears that sulfiding of the catalysts was rather extensive, since XRD did not show any residual CuO or other Cu species, even at the highest Cu loading (26%).

DISCUSSION

The results obtained in the present study can be interpreted on the basis of interactions between dispersed copper ions and the alumina support. Lo Jacono and Schiavello have reported that when divalent transition metal ions such as Cu, Co, and Ni are supported on alumina, formation of a "surface spinel" and/or bulk-like metal oxide occur, often concurrently (*1*). In these types of systems, impregnation of γ-Al_2O_3 with an aqueous metal salt, followed by drying and calcination, usually results in diffusion of metal ions into the support, forming an interaction species (i.e., a "surface spinel"). Formation of this interaction species has been previously confirmed using magnetic susceptibility (*3, 5, 6, 14*). DRS (*1, 3, 6, 9, 10, 14*), ESR (*3, 7, 8*), and EXAFS (*3*). Depending on the calcination temperature and time, only a finite amount of metal ions can be accommodated in the

vacant Oh and Td lattice sites of the support. Once all of the available lattice sites are saturated, further addition of metal ions can be accommodated only by segregation of a separate metal oxide phase. The results obtained in the present study are consistent with this general picture.

Nature of Surface Species

In our study, the Cu $2p_{3/2}$ ESCA binding energies for the catalysts varied with sample between values corresponding to CuO and $CuAl_2O_4$ (see Tables 2 and 3), indicating a surface having mixed species, or possibly the result of differential charging. Hence, ESCA binding energies could not be used to distinguish between CuO, $CuAl_2O_4$, or an interaction species. The Cu $2p_{3/2}$ satellite intensities were characteristic of bulk CuO, although XRD indicated that CuO was not present in a significant amount until Cu loadings of 13% of more. The similarity between the Cu $2p_{3/2}$ satellite intensities of bulk CuO and the catalysts (<13% CuO) does not necessarily mean that well-dispersed or amorphous CuO is present, but it does imply that the copper species is different from $CuAl_2O_4$. In fact that Cu/Al_2O_3 catalysts show lower reducibility than bulk CuO on heating under vacuum also suggests that the dispersed phase differs from CuO (*6, 14, 30*).

Although the ESCA results from the present study were inconclusive as to the nature of the interaction species, the PAS results were consistent with previous DRS studies, indicating the presence of octahedrally coordinated Cu(2+) ions on the catalysts (*3, 9*). Unfortunately, due to the limited range of the PAS spectrometer, the presence (or absence) of tetrahedrally coordinated Cu(2+) ions could not be confirmed. Hence, the exact nature of the interaction species could not be defined clearly, although it has previously been shown that in the "surface spinel," the Cu(2+) ions are predominantly (~90%) in a tetragonally distorted octahedral environment with some (~10%) tetrahedrally coordinated ions present (*3*). In contrast, the Cu(2+) distribution in bulk $CuAl_2O_4$ is 60% Td and 40% Oh (*3*) and in CuO is exclusively square planar (*3, 34*).

In discussing the nature of the copper–alumina interaction species, it is important to note, that bulk studies have shown that $CuAl_2O_4$ is thermodynamically unstable relative to CuO and Al_2O_3 at temperatures below 600–700°C (*3, 10, 33–35*). Table 7 lists the molar enthalpies of formation for several transition metal aluminates at 970 K (697°C) (*34*). Table 7 shows that among the first row transition metal aluminates, formation of $CuAl_2O_4$ is the least favorable (at ca. 700°C). However, at temperatures of 900–1000°C, formation of bulk $CuAl_2O_4$ becomes thermodynamically favorable (*10*), consistent with our bulk preparation (see Experimental). In fact, it is known that at 900°C, $CuAl_2O_4$ forms much more readily than either $NiAl_2O_4$ or $ZnAl_2O_4$ (*1*). In contrast to the thermodynamics of the preparation of bulk $CuAl_2O_4$, the "surface spinel" has been reported on Cu/Al_2O_3 catalysts under condition as mild as 300°C (*5*). Similarly, Lo Jacono and Schiavello (*1*) have reported that among the catalyst systems showing spinel formation (i.e., Cu/Al_2O_3, Co/Al_2O_3, and Ni/Al_2O_3), the copper "surface spinel" is the most readily formed. This should not be of too great concern, since the copper "surface spinel" differs in structure from bulk $CuAl_2O_4$, and the thermodynamics of highly dispersed phases are known to differ from bulk phases. Since the octahedrally coordinated "surface spinel" forms relatively easily, diffusion into tetrahedral sites is most likely the process which is thermodynamically limited, thus, preventing formation of a structure more like bulk $CuAl_2O_4$. At high calcination temperatures (>600°C), the diffusion of Cu(2+) ions from Oh sites to Td sites has also been found to be kinetically hindered (*3*).

In summary, our results indicate that, at low copper loadings (≤ca. 10%), Cu(2+) ions form a well-dispersed interaction species with the γ-Al_2O_3 support. The struc-

TABLE 7

Molar Enthalpies ($\Delta H°$) (kcal/mol) of Formation, Reduction, and Sulfidation for Transition Metal Aluminates at 970 K (697°C)

Compound	Formation[a] $MO + Al_2O_3 \rightarrow MAl_2O_4$	H_2 reduction[b] $MAl_2O_4 + H_2 \rightarrow M + Al_2O_3 + H_2O$	H_2S/H_2 sulfidation[b] $MAl_2O_4 + H_2S \rightarrow MS + Al_2O_3 + H_2O$
$CuAl_2O_4$	+5.2	−29.0	−33.5 (CuS); −66.2 (Cu_2S)[c]
$MnAl_2O_4$	−10.0	+43.4	−2.3
$FeAl_2O_4$	−10.8	+15.5	+1.6
$CoAl_2O_4$	−8.9	+5.4	+15.9 (Co_9S_8)[d]
$NiAl_2O_4$	−0.74	−2.2	−20.2
$ZnAl_2O_4$	−10.5	+35.4	−7.4

[a] Obtained from Ref. (*33*) (calorimetric measurements, reportedly ±0.3 kcal/mol or better).
[b] Estimated from thermodynamic data in Refs. (*33, 41*).
[c] $2\ CuAl_2O_4 + H_2S + H_2 \rightarrow Cu_2S + 2\ Al_2O_3 + 2\ H_2O$.
[d] $9\ CoAl_2O_4 + 8\ H_2S + H_2 \rightarrow Co_9S_8 + 9\ Al_2O_3 + 9\ H_2O$.

ture of this interaction species is different from both bulk CuO and $CuAl_2O_4$, with the Cu(2+) coordination being predominantly octahedral (tetrahedral Cu(2+) may or may not be present). At higher copper loadings, bulk-like CuO forms on the catalysts. The ESCA and ISS intensity ratio results are consistent with the general picture.

Dispersion and Location of Cu Species

The ESCA and ISS Cu/Al intensity ratios showed similar variations with metal content (see Figs. 4 and 5). Both plots showed an increase in the Cu/Al intensity ratio with increasing bulk copper content. However, there was a leveling off in the slope of the curves above approximately 9–10% Cu, indicating an alteration in surface composition. ESCA and ISS peak intensities from catalyst surfaces are influenced not only by surface concentration, but by factors such as surface area, pore size distribution and particle size. BET surface area measurements showed that variations in surface area among the catalysts were less than 20% between the highest and lowest Cu loadings. Hence, variation in surface area cannot account for the drastic changes in slope observed here.

Fung (*39*), and Kerkhof and Moulijn (*40*) have shown that, for supported metal catalysts having similar surface areas, the intensity ratio of ESCA peaks associated with the dispersed phase and the support will vary linearly with the dispersed-phase loading, provided that the size and shape of the supported particles do not vary significantly. Any deviation from linearity can be interpreted in terms of sample inhomogeneity or crystallite growth. Hence, the linear relationship from 0 to ca. 10% Cu seen in ESCA and ISS (see Figs. 4 and 5) indicates formation of a well dispersed Cu species of fairly constant particle size. This type of behavior would be expected for formation of an interaction type species where the Cu(2+) ions diffuse into the support with reasonably uniform distribution over the support surface. At some critical metal loading, the support becomes saturated and further addition of metal results in segregation of a separate metal oxide phase and crystallite growth. This phenomenon apparently occurs at ca. 9–10% Cu on the catalysts studied here.

It has been shown that, the total number of adsorption sites [for Cu(2+)] appears to be related generally to the surface area of the Al_2O_3 support. Friedman *et al.* reported results from various workers which indicated that for Cu/Al_2O_3 catalysts, saturation of the surface (i.e., monolayer cover-

age) occurs at a metal loading of approximately 4–5 wt% Cu per 100 m^2g^{-1} Al_2O_3 (*3*). Above this threshold loading, formation of crystalline CuO was observed. Similarly, Lo Jacono and Schiavello found that a copper "surface spinel" formed up to ca. 10 at.% Cu (unspecified surface area), above which, a CuO phase segregated (*1*).

Using Friedman's saturation value(s), "monolayer" coverage of the support used in this study (195 m^2/g) should occur at a copper content of approximately 8–10%. The break points of the ESCA and ISS curves occur at approximately 9–10% Cu (see Figs. 4 and 5) and therefore, can be attributed to saturation of the support. The appearance of diffraction lines characteristic of CuO in the XRD patterns of catalysts with higher loadings (i.e., ≥13% Cu) is consistent with support saturation. Once the support is saturated, agglomeration of copper species would occur, forming particles large enough to be detected by XRD (i.e., >50–75 Å). It is interesting to note that, a number of changes in catalyst properties appear to be correlated with the support capacity, i.e., magnetic susceptibility, CO adsorption, and catalytic activity (*3*).

The leveling off of the ESCA and ISS curves due to CuO particle growth can be rationalized by the fact that a greater volume of copper atoms becomes inaccessible to ESCA and ISS detection as the CuO particle size increases. Since the sampling depths of ESCA and ISS are on the order of 30 and 3 Å, respectively, atoms in the center of large particles cannot be detected. If less Cu is accessible to detection, the Cu/Al ESCA and ISS intensity ratios will level off. The suggested increase in CuO particle size with increasing metal loading is consistent with the XRD results shown in Table 1.

It was noted that at all concentrations, both the ESCA and ISS Cu/Al intensity ratios were lower for catalysts calcined at 600°C than for those calcined at 400°C (see Figs. 4 and 5). This effect is related to the extent of metal–support interaction, i.e., as the calcination temperature is increased, a greater percentage of copper ions diffuses into the γ-Al_2O_3 lattice. This effect has been demonstrated previously (*3*). If more copper ions diffuse into the support, the Cu/Al intensity ratios should be lower, exactly as observed by both ESCA and ISS.

Comparing Figs. 4 (ESCA) and 5 (ISS), ISS shows a much larger difference in the Cu/Al intensity ratio between the two calcination temperatures than does ESCA. This can be attributed to differences in sampling depths between ESCA and ISS. The larger difference seen in the ISS plot indicates that at constant Cu loading, the decrease in the amount of copper on the surface with increased calcination temperature is much greater over the sampling depth of ISS (ca. 3 Å), than it is over the sampling depth of ESCA (ca. 30 Å). This has important implications for catalysis since it is the uppermost layer of the catalyst surface that is involved in reactions. The results indicate that with increased calcination temperature, the uppermost surface layer is depleted of copper species to a greater extent than the outer 5–10 atomic layers, presumably due to increased diffusion of copper ions into the support. Hence, the catalytic activity should decrease for catalysts prepared at the higher calcination temperature (relative to those prepared at 400°C) to a greater extent than that expected from the ESCA data alone. This result demonstrates the great value of ISS in catalyst studies, since ISS has the unique ability to probe the uppermost surface layer.

Reactivity of Cu Species with H_2 and H_2/H_2S

The reduction and sulfidation experiments illustrate the high reactivity of Cu/Al_2O_3 catalysts, bulk CuO, and $CuAl_2O_4$ toward H_2 and H_2S/H_2. Hydrogen reduction of bulk CuO to Cu metal is thermodynamically favorable and known to occur readily (*6, 11, 14, 41*):

$$CuO + H_2 \rightarrow Cu + H_2O$$
$$\Delta H^\circ_{327°C} = -21.9 \text{ kcal/mol.}$$

Thermodynamic calculations (*42*) have shown that, under our experimental conditions, sulfidation of CuO to Cu_2S is also favorable:

$$2CuO + H_2S + H_2 \rightarrow Cu_2S + 2H_2O$$
$$\Delta H^\circ_{327°C} = -54.4 \text{ kcal/mol}$$

consistent with our experimental results. However, the fact that $CuAl_2O_4$ readily reduces and sulfides under relatively mild conditions is significant, since it is opposite to the behavior of similar aluminates of Co (*22, 36*), Ni (*11, 37*), Zn (*38*), and Mn (*43*), which are difficult to reduce and/or sulfide.

Molar enthalpies ($\Delta H°$) of reduction and sulfidation for a variety of transition metal aluminates were shown in Table 7. Thermodynamic data for the aluminates were available only for 970 K (697°C) (*34*). However, even though the reduction conditions employed in this and previous studies (*22, 36–38, 43*) were at lower temperatures (i.e., 400–500°C), the values shown in Table 7 are consistent with observed results and are useful for comparisons among the various systems.

Table 7 shows that among the aluminates listed, H_2 reduction is favorable only for $CuAl_2O_4$ and $NiAl_2O_4$. Previously, it has been shown that $CoAl_2O_4$, $ZnAl_2O_4$, and $MnAl_2O_4$ could not be reduced in hydrogen at temperatures of ca. 400–500°C (*22, 36, 38, 43*), consistent with Table 7. This low reactivity of transition metal aluminates has been attributed to the stability of divalent transition metal ions in Td spinel lattice sites (*22, 36*). $NiAl_2O_4$ is known to be difficult to reduce and is only partially reduced by H_2 (*11*), consistent with the low enthalpy of reduction (−2.2 kcal/mol). A kinetic effect may also account for the low reducibility of $NiAl_2O_4$. Our experimental results for H_2 reduction of $CuAl_2O_4$ are consistent with Table 7 and show that reduction to Cu metal occurs readily, even at 250–350°C.

The thermodynamics for H_2S/H_2 sulfidation of various aluminates are also consistent with our results and previous studies. Table 7 shows that H_2S sulfidation of $CuAl_2O_4$ to CuS is favorable; however, in the presence of H_2, sulfidation to Cu_2S is even more favored. This is consistent with our results which indicated formation of Cu_2S on sulfided $CuAl_2O_4$. Previously, it was shown that $CoAl_2O_4$ does not sulfide (*22*), and $ZnAl_2O_4$ (*38*) and $MnAl_2O_4$ (*43*) show only low reactivity toward H_2S/H_2 (500°C). Again, as in the reduction of these aluminates, kinetic effects probably also play an important role.

In comparison to bulk CuO and $CuAl_2O_4$, our results have shown that, Cu/Al_2O_3 catalysts readily undergo H_2 reduction (to Cu metal) and H_2S/H_2 sulfidation (to Cu_2S). Our results also indicate that the site symmetry of Cu(2+) ions (CuO—square planar; $CuAl_2O_4$—60% Td, 40% Oh; Cu/Al_2O_3 interaction species—predominantly Oh) has little effect on the reduction and sulfidation properties, in contrast to the Co/Al_2O_3 and Ni/Al_2O_3 systems (*36, 37*). Since both bulk CuO and $CuAl_2O_4$ are readily reduced and sulfided, the high reactivity of Cu/Al_2O_3 catalysts is not surprising, since the catalysts are composed of similar species (i.e., a copper/alumina interaction species which "resembles" $CuAl_2O_4$, although the structure differs somewhat, and/or bulk-like CuO).

CONCLUSIONS

Several conclusions can be drawn from this study:

(1) The surface characteristics of Cu/Al_2O_3 catalysts are affected by both metal loading and calcination temperature.

(2) For Cu/Al_2O_3 catalysts having low copper contents (<ca. 10%), copper ions from a well-dispersed interaction species with the support, which could not be detected by XRD. Results have indicated that the structure of this interaction species is different from bulk CuO and $CuAl_2O_4$. Although the structure of this interaction species is not clearly defined, PAS shows that

octahedrally coordinated Cu(2+) ions are present.

(3) At high copper loadings (after saturation of the support, i.e., >ca. 10% Cu), segregation of bulk-like CuO occurs, as detected by XRD. The crystallite size of this CuO phase increases with metal loading and calcination temperature.

(4) With increased calcination temperature, there is a depletion of copper on the catalyst surface due to increased diffusion into the support, as demonstrated by both ESCA and ISS.

(5) Cu/Al_2O_3 catalysts, as well as bulk CuO and $CuAl_2O_4$ are highly reactive toward H_2 reduction and H_2S/H_2 Sulfidation (350°C), forming Cu^0 and Cu_2S for the respective reactions.

(6) The comparative ESCA, ISS, XRD, and PAS results demonstrate the complementary nature and value of these techniques for the study of supported catalysts.

ACKNOWLEDGMENT

This work was partially supported by the National Science Foundation under Grant CHE-8108495.

REFERENCES

1. Lo Jacono, M., and Schiavello, M., *in* "Preparation of Catalysts" (B. Delmon, P. A. Jacobs, and G. Poncelet, Eds.), pp. 474–487. Elsevier, Amsterdam, 1976.
2. Pierron, E. D., Rashkin, J. A., and Roth, J. F., *J. Catal.* **9,** 38 (1967).
3. Friedman, R. M., Freeman, J. J., and Lytle, F. W., *J. Catal.* **55,** 10 (1978).
4. Ketchik, S. V., Plyasova, L. M., Seredkin, A. E., Kostrov, V. U., and Morozov, L. N., *React. Kinet. Catal. Lett.* **14**(4), 429 (1980).
5. Wolberg, A., and Roth, J. F., *J. Catal.* **15,** 250 (1969).
6. Hierl, R., Knözinger, H., and Urbach, H.-P., *J. Catal.* **69,** 475 (1981).
7. Berger, P. A., and Roth, J. F., *J. Phys. Chem.* **71**(13), 4307 (1967).
8. Deen, R., Th. Scheltus, P. I., and DeVries, G., *J. Catal.* **41,** 218 (1976).
9. Freeman, J. J., and Friedman, R. M., *J. Chem. Soc. Trans. Faraday* **1,** 758 (1978).
10. Lo Jacono, M., Cimino, A., and Inversi, M., *J. Catal.* **76,** 320 (1982).
11. Bailey, G. W., and Wade, J. T., *Thermochim. Acta* **8,** 149 (1974).
12. Chen, H. C., and Anderson, R. B., *J. Catal.* **43,** 200 (1976).
13. Wolberg, A., Ogilvie, J. L., and Roth, J. F., *J. Catal.* **19,** 86 (1970).
14. Ertl, G., Hierl, R., Knözinger, H., Thiele, N., and Urbach, H.-P., *Appl. Surf. Sci.* **5,** 49 (1980).
15. Barber, M., Sharpe, P. K., and Vickerman, J. C., *J. Catal.* **41,** 240 (1976).
16. Shelef, M., Wheeler, M. A. Z., and Yao, H. C., *Surf. Sci.* **47,** 697 (1975).
17. Holgersson, S., *Z. Anorg. Allg. Chem.* **204,** 378 (1932).
18. Burggraf, L. W., and Leyden, D. E., *Anal. Chem.* **53,** 759 (1981).
19. Klug, H. P., and Alexander, L. E., "X-Ray Diffraction Procedures for Polycrystalline and Amorphous Materials," 2nd ed. Wiley, New York, 1974.
20. Ng, K. T., and Hercules, D. M., *J. Phys. Chem.* **80,** 2094 (1976).
21. Patterson, T. A., Carver, J. C., Leyden, D. L., and Hercules, D. M., *J. Phys. Chem.* **80,** 1700 (1976).
22. Chin, R. L., and Hercules, D. M., *J. Phys. Chem.* **86,** 3079 (1982).
23. Burggraf, L. W., Leyden, D. E., Chin, R. L., and Hercules, D. M., *J. Catal.* **78,** 360 (1982).
24. Wagner, C. D., *Anal. Chem.* **47,** 1201 (1975).
25. Fiermans, L., Hoogewijs, R., and Vennik, J., *Surf. Sci.* **47,** 1 (1975).
26. Scrocco, M., *Chem. Phys. Lett.* **63,** 52 (1979).
27. Wallbank, B., Johnson, C. E., and Main, I. G., *J. Electron Spectrosc. Relat. Phenom.* **4,** 263 (1974).
28. Rosencwaig, A., and Wertheim, G. K., *J. Electron Spectrosc. Relat. Phenom.* **1,** 493 (1972).
29. Klein, J. C., Li, C. P., Hercules, D. M., and Black, J. F., submitted for publication.
30. Strohmeier, B. R., unpublished studies, University of Pittsburgh, 1984.
31. Herman, R. G., Klier, K., Simmons, G. W., Finn, B. P., Bulko, J. B., and Kobylinski, T. P., *J. Catal.* **56,** 407 (1979).
32. Hosotsubo, T., Sugioka, M., and Aomura, K., *Bull. Fac. Eng. Hokkaido Univ.* **102,** 119 (1981).
33. Navrotsky, A., and Kleppa, O. J., *J. Inorg. Nucl. Chem.* **29,** 2701 (1967).
34. Navrotsky, A., and Kleppa, O. J., *J. Inorg. Nucl. Chem.* **30,** 479 (1968).
35. Jacob, K. T., and Alcock, C. B., *J. Amer. Ceram. Soc.* **58,** 192 (1975).
36. Chin, R. L., and Hercules, D. M., *J. Phys. Chem.* **86,** 360 (1982).
37. Wu, M., and Hercules, D. M., *J. Phys. Chem.* **83,** 2003 (1979).

38. Strohmeier, B. R., and Hercules, D. M., *J. Catal.* **86,** 266 (1984).

39. Fung, S. C., *J. Catal.* **58,** 454 (1979).

40. Kerkhof, F. P. J. M., and Moulijn, J. A., *J. Phys. Chem.* **83,** 1612 (1979).

41. Okamoto, Y., Fukino, K., Imanaka, T., and Teranishi, S., *J. Phys. Chem.* **87,** 3747 (1983).

42. Barin, I., and Knacke, O., "Thermochemical Properties of Inorganic Substances." Springer-Verlag, New York, 1973.

43. Strohmeier, B. R., and Hercules, D. M., *J. Phys. Chem.* **88,** 4922 (1984).

44. Scofield, J. H., *J. Electron Spectrosc. Relat. Phenom.* **8,** 129 (1976).

45. Wheeler, M. A., *Anal. Chem.* **47,** 146 (1975).